SCIENCE CHINA
Earth Sciences

•ARTICLE•

https://doi.org/10.1007/s11430-024-1502-y

Impact of net-zero emissions on atmospheric CO_2 concentration in China: Ideal simulations based on the GEOS-Chem model

Jingye TAN[1,2], Jun WANG[1,2*], Huiqin MAO[3], Hengmao WANG[1,2], Zhiqiang LIU[4], Meirong WANG[5,6], Ran YAN[1,2], Xunmei WANG[1,2] & Fei JIANG[1,2]

[1] *Frontiers Science Center for Critical Earth Material Cycling, International Institute for Earth System Science, Nanjing University, Nanjing 210023, China*

[2] *Jiangsu Provincial Key Laboratory of Geographic Information Science and Technology, Key Laboratory for Land Satellite Remote Sensing Applications of Ministry of Natural Resources, School of Geography and Ocean Science, Nanjing University, Nanjing 210023, China*

[3] *Satellite Environmental Application Center, Ministry of Environmental Protection, Beijing 100094, China*

[4] *CMA Key Open Laboratory of Transforming Climate Resources to Economy, Chongqing Institute of Meteorological Sciences, Chongqing 401147, China*

[5] *State Key Laboratory of Climate System Prediction and Risk Management, Key Laboratory of Meteorological Disaster, Ministry of Education, Collaborative Innovation Center on Forecast and Evaluation of Meteorological Disasters, Nanjing University of Information Science and Technology, Nanjing 210044, China*

[6] *Xizang Field Station for Scientific Observation and Research on Atmospheric Water Cycle in Mêdog, Xigazê and Mêdog National Climate Observatory, Xizang Meteorological Service, Lhasa 850000, China*

Received June 1, 2024; revised November 8, 2024; accepted December 26, 2024; published online February 11, 2025

Abstract Elevated atmospheric carbon dioxide (CO_2) concentrations have caused global climate change such as global warming and more frequent climate extremes. Countries worldwide have proposed carbon neutrality strategies to curb the rising CO_2 concentrations. To investigate the impact of China's carbon neutrality goal on atmospheric CO_2 concentrations, we conducted a series of ideal simulations from 2015 to 2019 using a global 3D chemistry transport model, Goddard Earth Observing System Chemistry (GEOS-Chem). Compared with the column-averaged dry-air mole fraction of atmospheric CO_2 (XCO_2) from Orbiting Carbon Observatory-2 (OCO-2) and surface CO_2 measurements in ObsPack, we find that GEOS-Chem effectively reproduces the spatiotemporal variability of CO_2. The model exhibits a root mean square error (RMSE) of 1.51 ppm (R^2=0.89) for OCO-2 XCO_2 in China and 2.65 ppm (R^2=0.75) for surface CO_2 concentrations at the WLG station. Further, compared to 2.83 ppm yr^{-1} in the control experiment, we suggest that net-zero CO_2 emissions in China decelerate the increasing trends of XCO_2 to 1.81 ppm yr^{-1}, making a decrease of approximately 35.89%. Meanwhile, the seasonal cycle amplitude (SCA) of XCO_2 is moderately reduced from 7.39±0.81 to 6.75±0.70 ppm, representing a relative reduction of 9.91%. Spatially, net-zero CO_2 emissions induce a more significant decrease in XCO_2 trends over northern and southern China, while their impact on SCA is more evident in northern and northeastern China. Moreover, ideal experiments demonstrate that zero fossil CO_2 emissions lead to a greater attenuation of the linear trends of XCO_2 by 40.81%, while the absence of terrestrial CO_2 sinks largely diminishes the SCA by 16.61%. Additionally, trends and SCA in surface CO_2 concentrations exhibit almost identical decreasing responses to net-zero CO_2 emissions but display greater sensitivities compared to XCO_2. Overall, our study underscores the potential of China's carbon neutrality goal in mitigating global warming, underscoring the need for concerted and collaborative efforts from nations worldwide.

Keywords XCO_2, GEOS-Chem, Carbon neutrality, Net-zero emissions, Surface CO_2 concentrations

Citation: Tan J, Wang J, Mao H, Wang H, Liu Z, Wang M, Yan R, Wang X, Jiang F. 2025. Impact of net-zero emissions on atmospheric CO_2 concentration in China: Ideal simulations based on the GEOS-Chem model. Science China Earth Sciences, 68, https://doi.org/10.1007/s11430-024-1502-y

* Corresponding author (email: wangjun@nju.edu.cn)

1. Introduction

Continued greenhouse gas emissions, primarily from human activities such as fossil fuel combustion and cement manufacturing (Höök and Tang, 2013; He et al., 2022), have notably elevated atmospheric carbon dioxide (CO_2) concentrations from pre-industrial levels of 280 ppm (1 ppm=1 μg g^{-1}) to approximately 417.9 ppm in 2022 (WMO, 2023). The increase in atmospheric CO_2 has intensified the greenhouse effect, contributing to global warming with a surface temperature increase of 1.07°C (IPCC, 2021; Jeffry et al., 2021; Ponce and Khan, 2021). Consequently, it has increased the frequency and intensity of extreme weather events and compound hazards (Agha-Kouchak et al., 2020; Laufkötter et al., 2020; Gampe et al., 2021), such as heatwaves, droughts, wildfires, precipitation, and floods, posing a threat to human health, economic stability, and ecological balance (Zhang and Zhou, 2020; Vicedo-Cabrera et al., 2021).

Currently, atmospheric CO_2 concentrations are monitored and studied using three main methods: satellite space-based monitoring, ground station observation, and model simulations (Jin et al., 2022). Satellite space-based monitoring offers a global perspective of the seasonal cycle and spatial patterns of atmospheric CO_2 with sufficient accuracy, coverage, and resolution. Data on the column-averaged dry-air mole fraction of atmospheric CO_2 (XCO_2) data generated by the Greenhouse Gases Observing Satellite (GOSAT), the Orbiting Carbon Observatory-2 (OCO-2), and the Orbiting Carbon Observatory-3 (OCO-3) are widely used in studies of atmospheric CO_2 concentration variations (Chatterjee et al., 2017; Eldering et al., 2017; Wang et al., 2020; Li et al., 2022; Feldman et al., 2023). Ground-based observations, such as the Total Carbon Column Observing Network (TCCON) and the Observation Package framework (ObsPack), provide accurate measurements of ground-level CO_2 concentrations. However, the limited number of ground-based stations constrains comprehensive analysis of ground-level concentrations (Zhang et al., 2017). While spaceborne and ground-based observations effectively track changes in atmospheric CO_2 concentration, they cannot differentiate between anthropogenic and natural emission sources. This limitation can be addressed by the model simulation method, which controls and constrains the input data. For instance, models like the Goddard Earth Observing System Chemistry global 3D chemistry transport model (GEOS-Chem) play a crucial role in this regard (Messerschmidt et al., 2013; Allahudheen et al., 2023).

In an effort to mitigate the global warming, nations signed *The Paris Agreement*, which aims to limit global temperature rise to well below 2°C and seeks to limit warming to 1.5°C (Rogelj et al., 2016; Roelfsema et al., 2020). In order to realize this vision, CO_2 emissions need to achieve a balance between anthropogenic emissions by sources and removals by sinks, which is known as net-zero emissions or carbon neutrality (Fuglestvedt et al., 2018; Rogelj et al., 2019). In this regard, more than 100 countries have or are considering achieving net-zero emissions or neutralization targets (van Soest et al., 2021). For example, the United States and the European Union both plan to achieve net zero greenhouse gas emissions by 2050 (Salvia et al., 2021; Williams et al., 2021). China, a major emitter of greenhouse gases, accounts for approximately 10%±4% of the current global radiative forcing, with CO_2 emissions from fossil fuel burning being its largest contributor, estimated at 0.16±0.02 W m^{-2} (Li et al., 2016). In order to achieve those targets of *the Paris Climate Agreement*, China has proposed implementing more stringent policies and measures to ensure CO_2 emissions achieve carbon peak and carbon neutrality in this century at the general debate of the 75th session of the United Nations General Assembly (Zhang et al., 2021; Dong et al., 2022).

Existing research on net-zero emissions has primarily focused on pathways and strategies from technical and policy perspectives, such as energy transition, and Carbon Capture, Utilization, and Storage (CCUS) (Chen et al., 2022; Shang and Lv, 2023). Most analyses of atmospheric CO_2 concentrations have emphasized their spatial distribution and temporal changes (Keenan et al., 2016; Su et al., 2023; Liu et al., 2024; Lou et al., 2024). However, the impact of regional net-zero emissions, such as in China, on atmospheric CO_2 concentrations and the extent of reduction remain unclear. In this study, we will employ the GEOS-Chem model to perform an ideal simulation to examine the changes in XCO_2 and surface CO_2 concentrations under net-zero emissions conditions. Our analysis will focus on variations in their trends and the amplitudes of the seasonal cycle. Additionally, we will conduct sensitivity experiments to quantitatively assess the individual effects of regional fossil CO_2 emissions and terrestrial CO_2 sinks on XCO_2.

2. Datasets and methods

2.1 OCO-2 XCO_2 product

We employed spaceborne measurements of atmospheric XCO_2 obtained from OCO-2 satellite launched in July 2014. The OCO-2 project comprises three high-resolution spectrometers that simultaneously measure reflected sunlight in the near-infrared CO_2 bands near 1.61 and 2.06 μm, as well as in the molecular oxygen A-band at 0.76 μm. OCO-2 crosses the equator at 1:36 p.m. local time, with the cycle for a near repeat of observations of 16 d or 233 orbits. OCO-2 carried out observations in three modes of nadir, glint, and target. After the first year, alternating nadir/glint observations are carried out on all orbits except for scintillation

observations over the majority of the Pacific and Atlantic Oceans. Specifically, we use the OCO2_L2_Lite_FP dataset version 11 (Kiel et al., 2019), characterized by a spatial resolution of 2.25 km×1.29 km. The dataset used in this study covers the time period from January 1, 2015 to December 31, 2019, with data gaps observed between August 1, 2017 and September 18, 2017. In this study, the XCO_2 data did not differentiate between nadir and glint observation methods, selecting data with a quality flag of "good quality" (QA=0). To align with the horizontal resolution of the GEOS-Chem model, we mapped the satellite data onto a consistent 2°×2.5° latitude/longitude grid, by averaging observations within each grid cell.

2.2 Surface CO_2 from ObsPack

We utilized CO_2 surface observations sourced from the ObsPack data products (Masarie et al., 2014; Schuldt et al., 2022). The ObsPack framework consolidates atmospheric greenhouse gas observations from various sampling platforms, modeled on the collaborative GLOBALVIEW product initiated in 1996 to aid carbon cycle modeling studies. There were only 10 stations within China, and after excluding marine and border areas, data were available for just 6 stations: WLG, LFS, LAN, XGL, JSA, and SDZ stations. We selected four of these in the main text based on their orientation, vegetation cover, and anthropogenic emission intensity, and the others (JSA and SDZ) are in Appendix Figure S1 (https://link.springer.com). Detailed locations (latitudes and longitudes) and observation time information for these stations are provided in Table 1 and Figure 1b. We used these four stations as representatives of the surface CO_2 concentrations in various regions of China, namely, WLG station for western China, LFS station for northern China, LAN station for eastern China, and XGL station for southwestern China.

2.3 GEOS-Chem model and its simulation experimental designs

The GEOS-Chem model enables the simulation of atmospheric CO_2 concentration on a broad scale across both space and time. For this study, we used GEOS-Chem version 13.2.0, which integrates archived GEOS weather data on a linear latitude and longitude grid to calculate horizontal and vertical transport processes (Bukosa et al., 2023). The meteorological driving fields are sourced from MERRA-2 reanalysis data, featuring a 3-h temporal resolution for 3D fields and a 1-h resolution for 2D fields. To initialize the model, we conducted a one-year spin-up restarting from an assimilation study (Wang et al., 2019) to generate the required restart file dated 2015-01-01 for our study. The model outputs time-averaged data hourly and generates a file monthly. All other parameters were set to default.

For our atmospheric CO_2 concentration simulations, we took some emission data from the Harmonized Emissions Component (HEMCO) version 3.5.0 (Keller et al., 2014; Lin et al., 2021). Specifically, we sourced fossil fuel emissions from the Open-source Data Inventory for Anthropogenic CO_2 (ODIAC) (Oda and Maksyutov, 2011), ship emissions from the Common Education Data Standards (CEDS) (Hoesly et al., 2018), aircraft emissions from Aircraft Emissions Inventory Code 2019 (AEIC 2019) (Olsen et al., 2013), and open fire emissions from Global Fire Emissions Database 4.1s (GFED 4.1s) (Randerson et al., 2018). In addition, we utilized land and ocean carbon sources and sinks obtained from the posterior product optimized by the Global Carbon Assimilation System version 2 (GCASv2) (Jiang et al., 2021). Figure 1 shows the annual average values for fossil CO_2 emissions and terrestrial CO_2 sinks in 2015. It highlights China's significant contribution, representing approximately 27.8% of global fossil CO_2 emissions, totaling 9.68 Gt CO_2, and 23.0% of global terrestrial CO_2 sinks, sequestering 1.68 Gt CO_2. This underscores the crucial role of both China's fossil CO_2 emissions and terrestrial CO_2 sinks in the global carbon budget.

In order to further investigate the impact of achieving net-zero carbon emissions on XCO_2 in China and to better understand the individual contributions of fossil CO_2 emissions and terrestrial CO_2 sinks, we designed the following four experiments. They included a control experiment (referred to as CTL) and three sensitivity experiments (referred to as EXP1, EXP2, and EXP3, respectively).

(1) CTL: All emissions are used normally from 2015 to 2019.

(2) EXP1: The total carbon fluxes of fossil CO_2 emissions and terrestrial CO_2 sinks in China are set to zero from 2015 to 2019.

(3) EXP2: Only fossil CO_2 emissions are set to zero in China from 2015 to 2019.

(4) EXP3: Only terrestrial CO_2 sinks are set to zero in China from 2015 to 2019.

Thus, EXP1-CTL can elucidate the impact of China's net CO_2 emissions on XCO_2 under ideal net-zero emission conditions. Meanwhile, EXP2-CTL and EXP3-CTL delineate the effects of China's fossil CO_2 emissions and terrestrial CO_2 sinks, respectively, on XCO_2 variations. The output of these experiments consists of 72-layer CO_2 concentration data with a spatial resolution of 2°×2.5° (latitude×longitude) and a temporal resolution of 1 h. To facilitate direct comparison with satellite-observed XCO_2 data, a transformation of the 72-layer CO_2 concentration into XCO_2 is imperative.

Since the GEO-Chem uses the hybrid sigma-pressure coordinate system vertically, we first calculated the actual air pressure value corresponding to the center point of each layer based on the surface atmospheric pressure from MERRA-2.

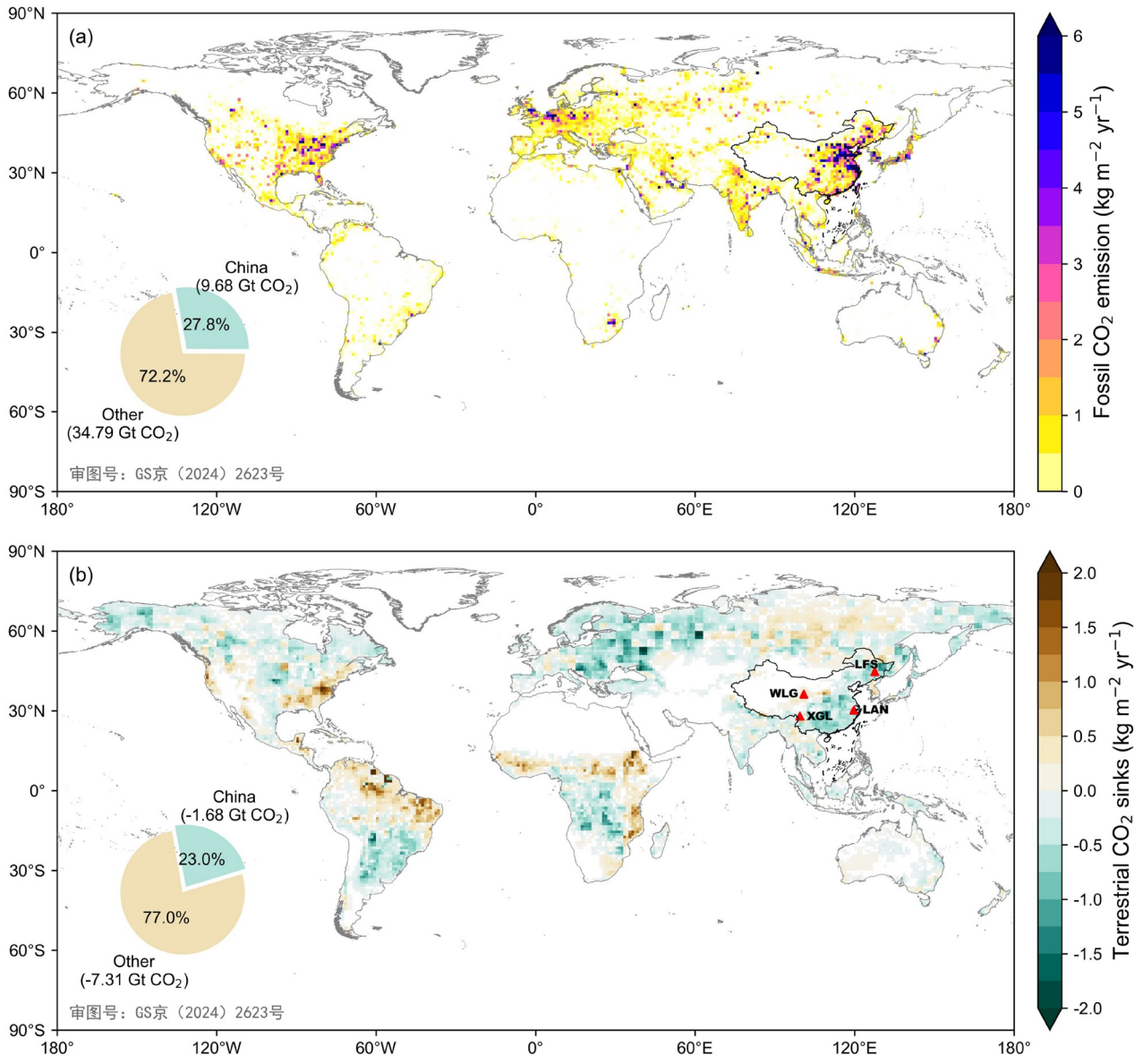

Figure 1 Input data for fossil CO_2 emissions and terrestrial CO_2 sinks in 2015. (a) The annual average fossil CO_2 emissions from ODIAC in 2015; (b) the annual average terrestrial CO_2 sinks from GCAS in 2015. Additionally, the red triangles in (b) indicate the locations of the used ObsPack stations in this study.

Table 1 Information for the observation stations used in this study

Station	Latitude, longitude	Start date	Stop date	Province
WLG	36.29°N, 100.90°E	1990-08-05	2021-12-29	Qinghai
LFS	44.73°N, 127.60°E	2009-01-01	2016-12-31	Heilongjiang
LAN	30.30°N, 119.73°E	2009-01-02	2016-12-31	Zhejiang
XGL	28.01°N, 99.44°E	2010-08-02	2016-12-31	Yunnan

Then, we interpolated the simulated CO_2 concentration results from the 72 layers of GEO-Chem model to the 20 layers of OCO-2 based on the air pressure. Finally, we obtained modeled XCO_2 based on the apriori CO_2 profile, column averaging kernel, and pressure weights of OCO-2 (Connor et al., 2008). Specifically, we computed the GEOS-Chem modeled XCO_2 as follows:

$$XCO_2 = pXCO_2 + \sum_j \left(h_j A_j \left(X_m - X_p \right)_j \right), \quad (1)$$

where $pXCO_2$ represents the XCO_2 apriori value, h_j represents the pressure weights, A_j represents the column

averaging kernel. X_m and X_p represent the GEO-Chem simulation value and the CO_2 priori profile, respectively. And j denotes the levels (20 layers).

2.4 Curve fitting for atmospheric CO_2 concentration

Changes in atmospheric CO_2 concentration primarily consist of short-term fluctuations, seasonal cycle, interannual and decadal variations, and long-term trends. To analyze the trends and seasonal cycle of CO_2 concentrations, we for simplicity decompose the time series using a curve-fitting method (Press et al., 1988; Thoning et al., 1989). The function applied in this study is presented as:

$$f(t) = a_0 + a_1 t + \sum_{n=1}^{4} c_n[\sin(2n\pi t + \varphi_n)], \quad (2)$$

where the constant term a_0 represents the background concentration of XCO_2 during the study period. The coefficient of the primary term a_1 signifies the linear trends, i.e., the long-term growth rate of XCO_2, while the remaining harmonic terms are related to the seasonal cycle. c_n is the harmonic term coefficient, and harmonics of a yearly cycle represents the annual oscillation. The function fits the data based on the methods of general linear least squares regression and determines a_0, a_1, and c_n. In this study, we calculated the seasonal cycle amplitude (SCA) by averaging the differences between the peak and trough of the harmonic term amplitude across multiple years. Meanwhile, the trend of time series was the polynomial part of the function plus the long-term filter of the residuals.

3. Results

3.1 Model performance

To better understand the impact of net-zero CO_2 emissions on China's CO_2 concentration, we evaluated the performance of GEOS-Chem model simulations (Figure 2). OCO-2 satellite observations of XCO_2 reveal a noticeable upward trend from 398 ppm in 2015 to 412 ppm in 2019 over China, exhibiting a trend slope of 2.60 ppm yr^{-1} (p<0.01). Additionally, satellite-observed XCO_2 exhibits a distinct seasonal cycle, with a peak in April and a minimum in August, demonstrating a SCA of 8.78±0.67 ppm. This variation is due to ecosystems absorbing CO_2 in the summer when photosynthesis exceeds respiration, and releasing CO_2 in the winter when respiration dominates. The GEOS-Chem modeled XCO_2 also shows a significant upward trend of 2.83 ppm yr^{-1} (p<0.01) and a clear seasonal cycle, with the SCA of 7.39±0.70 ppm, consistent with the OCO-2 observations. Comparing the GEOS-Chem simulated and OCO-2 observed XCO_2, their relationship closely aligns with the 1:1 line with an actual slope of 0.95, showing their root mean square error (RMSE) of 1.51 ppm and a coefficient of determination (R^2) of 0.89. It highlights the strong agreement between the modeled and observed XCO_2 concentrations.

Furthermore, we conducted a comparison between the GEOS-Chem simulated near-surface CO_2 concentration and surface observations from ObsPack at four *in-situ* stations (Figure 3). At WLG station, which serves as an atmospheric background baseline monitoring site, a clear upward trend in CO_2 concentration (2.51 ppm yr^{-1}, p<0.01) is observed, accompanied by a pronounced seasonal cycle similar to satellite-observed XCO_2. The comparison between simulated and observed surface CO_2 shows RMSE of 2.65 ppm and R^2 of 0.75. Conversely, at LFS, LAN, and XGL stations, the surface CO_2 concentrations do not exhibit clear trends due to the short duration of observations, all ending in December 2016. Nonetheless, a strong seasonal cycle is evident at LFS stations, with RMSE of 7.82 ppm (R^2=0.70). The LAN station, located in the Yangtze River Delta region, reflects more pronounced effects of fossil CO_2 emissions, resulting in a

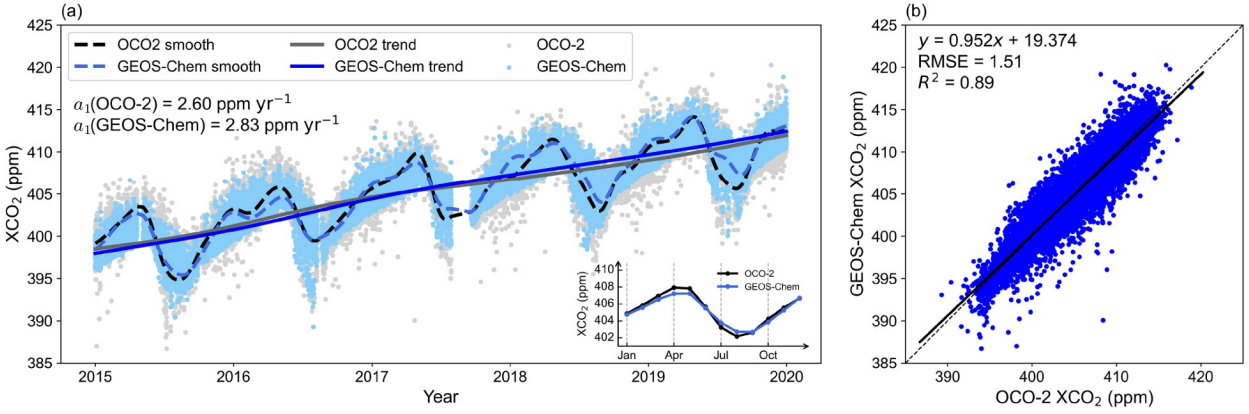

Figure 2 Comparison between GEOS-Chem simulated and OCO-2 observed XCO_2 in China. (a) Time series of OCO-2 observations (grey dots and black lines) and the GEOS-Chem simulations (blue dots and lines). Their original values are shown in dots, with the smoothed fitted curves in dashed lines, and the trends in solid lines. The inserted subplot represents the seasonal cycle of OCO-2 observations (the black line) and the GEOS-Chem simulations (the blue line), with monthly XCO_2 as a multi-year monthly average. (b) Scatter plots for the observed and simulated XCO_2. The unit of XCO_2 is in ppm.

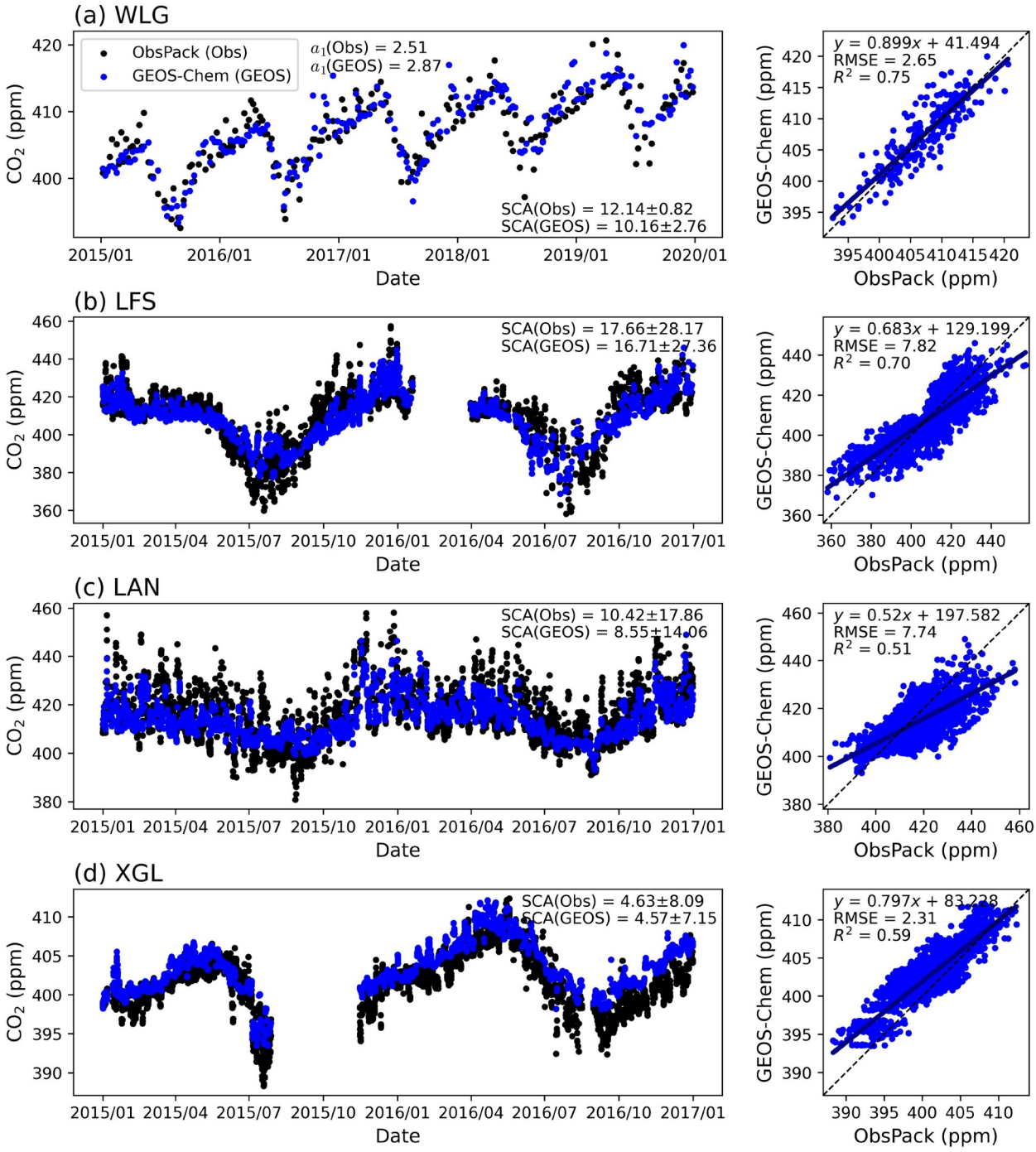

Figure 3 Comparison between GEOS-Chem simulated and station-observed surface CO_2 concentration at WLG (a), LFS (b), LAN (c), and XGL (d). The left column shows the time series of GEOS-Chem simulated results (blue dots) and ObsPack observations (black dots). The right column shows the relationship between the observed and simulated CO_2 concentrations. The unit of a_1 is ppm yr^{-1} and the unit of SCA is ppm.

weaker seasonal cycle with a RMSE of 7.74 ppm (R^2=0.51). Meanwhile, XGL, located in the southwestern mountainous area, exhibits the weakest SCA of 4.63±8.09 ppm, suggesting RMSE of 2.31 ppm (R^2=0.59). Overall, GEOS-Chem basically demonstrates reasonable performance in simulating surface CO_2 concentrations, although with larger RMSE compared to XCO_2.

3.2 Impact of ideal net-zero CO_2 emissions

Figure 4 shows the changes in XCO_2 in China under the ideal net-zero CO_2 emissions (EXP1) relative to the CTL simulation. Clearly, we can find that the simulated results in EXP1 show a remarkably significant decrease in trend. Quantitatively, the linear trend in EXP1 is 1.81 ppm yr^{-1}

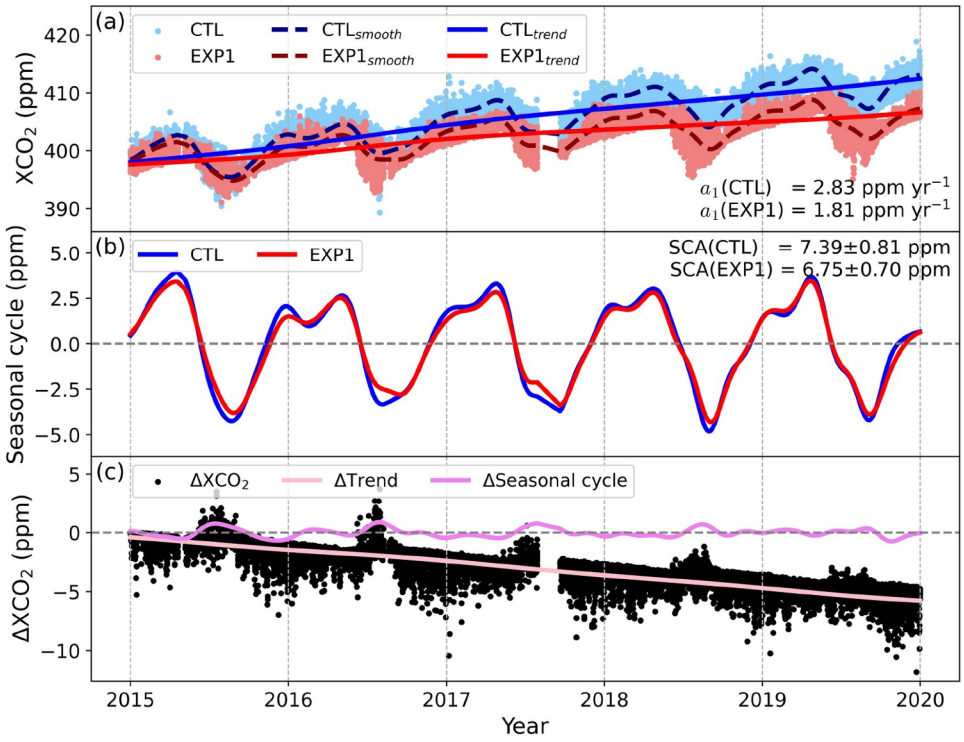

Figure 4 XCO_2 changes in China under ideal net-zero carbon emissions. (a) The original XCO_2 (dots), smoothed fitted curves (dashed lines), and trend lines (solid lines) of XCO_2 in the control simulation (CTL, blue dots and lines) and ideal net-zero emission experiment (EXP1, red dots and lines); (b) seasonal cycle of XCO_2 in CTL (blue line) and EXP1 (red line); (c) difference in XCO_2 between EXP1 and CTL, including original values (black dots), trends (pink line), and seasonal cycles (purple line).

(p<0.01), compared to 2.83 ppm yr^{-1} (p<0.01) in CTL, representing a decrease of 1.02 ppm yr^{-1}. In other words, approximately 64% of the increasing XCO_2 trend in China is induced by CO_2 emissions outside China transported by atmospheric circulations. The cumulative amount of XCO_2 under net-zero CO_2 emissions is reduced by 5.39 ppm over the course of 5 years, which is smaller than China's cumulative CO_2 emissions from fossil fuels, amounting to 6.15 ppm (approximately 47.85 Gt CO_2). In contrast, the change in the SCA of XCO_2 is less pronounced with 6.75±0.70 ppm in EXP1 compared to 7.39±0.81 ppm in CTL, suggesting that China's carbon sources and sinks have a weaker influence on its SCA of XCO_2. Overall, the combined effect of China's net-zero CO_2 emissions from fossil CO_2 emissions and terrestrial CO_2 sinks would reduce the linear trends of XCO_2 by approximately 35.89%, and diminish the SCA over China by approximately 9.91% (Table 1).

Spatially, the impact of China's net-zero CO_2 emissions is evident in the regional trends of XCO_2, with widespread decreasing trends observed (Figure 5a). Specifically, stronger reductions in XCO_2 trends are observed over northern and southern China, while the weakest reductions happen over the Tibetan Plateau. Interestingly, this pattern differs from the spatial distributions of fossil CO_2 emissions and terrestrial CO_2 sinks in China (Figures 1 and 5a). It is most probably due to the influence of atmospheric circulations, such as the East Asian monsoon (Appendix Figure S2). For instance, strong fossil CO_2 emissions over North China can be greatly transported into Central China by prevailing northeasterly winds in winter (Appendix Figures S2–S4). Consequently, although local fossil CO_2 emissions are weak over Central China, reductions in XCO_2 trends are most pronounced in this region. This phenomenon is further supported by year-by-year relative changes (Appendix Figure S4a–S4e).

Similarly, changes in the SCA of XCO_2 display heterogeneity in its spatial distribution (Figure 5b). In detail, the SCA in Northern and Northeastern China experiences a more significant decrease, while slight changes in the SCA occur in southern China under net-zero emissions. These changes in the SCA of XCO_2 are closely related to the seasonal cycle of terrestrial CO_2 sinks. In winter, weak carbon sources are observed in northern and northeastern China, while strong carbon sinks are present in summer (Appendix Figure S5), suggesting pronounced seasonal variations in these regions, which correspond well to the locations showing strong changes in the SCA of XCO_2 (Figure 5b). In contrast, southern China shows carbon sequestration throughout the year, resulting in relatively weak

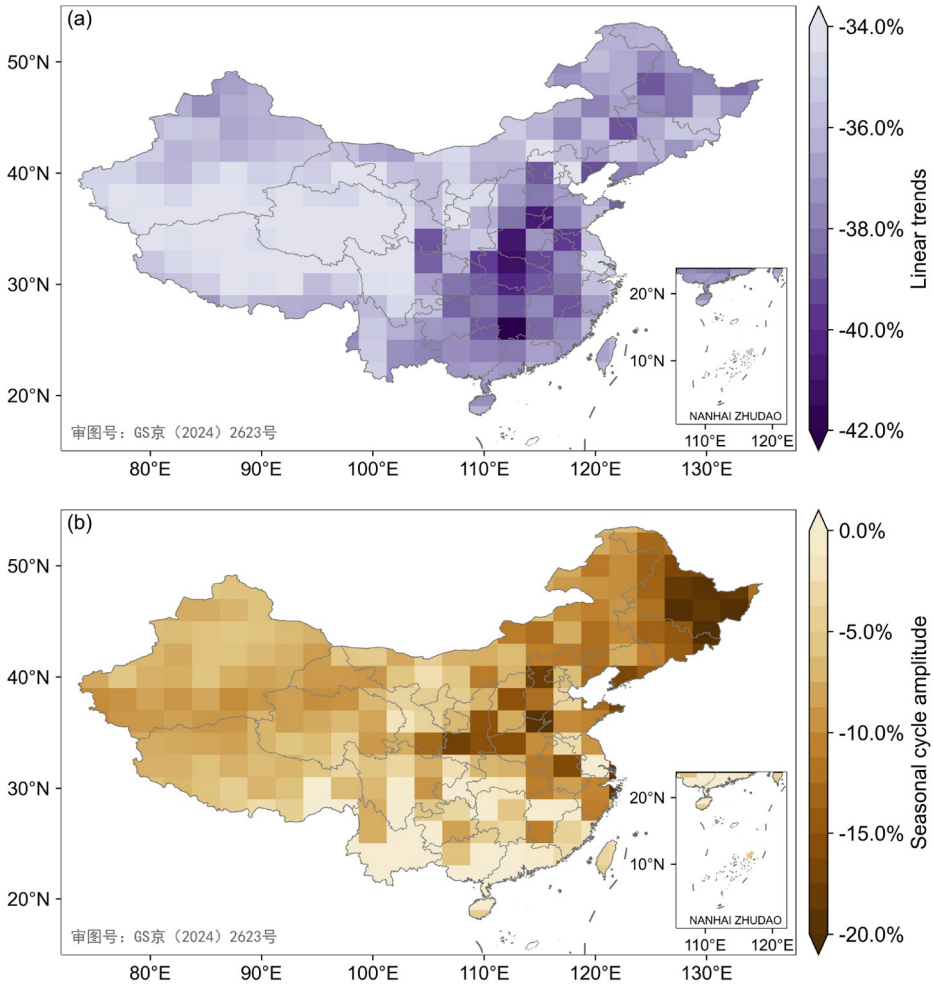

Figure 5 Relative changes in trends and seasonal cycle amplitude (SCA) of XCO_2 in China between EXP1 and CTL. (a) Relative changes in trends in China; (b) relative changes in the SCA of XCO_2.

changes in the SCA of XCO_2. Additionally, in western China where there is no significant seasonal difference in CO_2 sinks, the SCA of XCO_2 is reduced to some extent under net-zero emissions, which is due to modulations in atmospheric circulations.

3.3 Individual contributions of fossil CO_2 emissions and terrestrial CO_2 sinks to XCO_2 variations

We conducted further analysis to assess the individual impacts of surface CO_2 fluxes from fossil CO_2 emissions and terrestrial CO_2 sinks in China. Utilizing the results from the experiment (EXP2) with zero anthropogenic fossil CO_2 emissions, we find that the linear trends of XCO_2 is 1.67 ppm yr^{-1} (p<0.01), with a corresponding SCA of 7.95±1.34 ppm (Figure 6). Compared with those values obtained in the CTL of 2.83 ppm yr^{-1} (p<0.01) and 7.39±0.81 ppm, respectively, the linear trends of XCO_2 in China decreases by 1.16 ppm yr^{-1}, while the SCA show a slight increase of 0.59 ppm. Consequently, without fossil CO_2 emissions, the linear trends of XCO_2 can be reduced by approximately 40.81%, whereas the SCA increases slightly by about 7.57% (Table 2). These findings highlight the dominant role of changes in fossil CO_2 emissions in driving the reductions in the increasing trends of XCO_2 in the context of ideal net-zero CO_2 emissions.

Figure 6d and 6e show the spatial patterns of changes in trends and the SCA of XCO_2 in China under EXP2 relative to CTL, respectively. Notably, without fossil CO_2 emissions, the reductions in linear trends of XCO_2 are significantly stronger, even surpassing −46% in certain regions, and exhibiting a spatial pattern closely resembling that under net-zero CO_2 emissions (Figures 6d and 5a). Conversely, the SCA strengthens, especially over the southwestern regions (Figure 6b). Compared with Eastern China, where XCO_2 declines sharply throughout the year, Southern China has a smaller decline in XCO_2 in the spring and a large decline in the other seasons (Appendix Figure S6), making the effect of zero fossil CO_2 emissions on the SCA of XCO_2 in Southwestern China more significant.

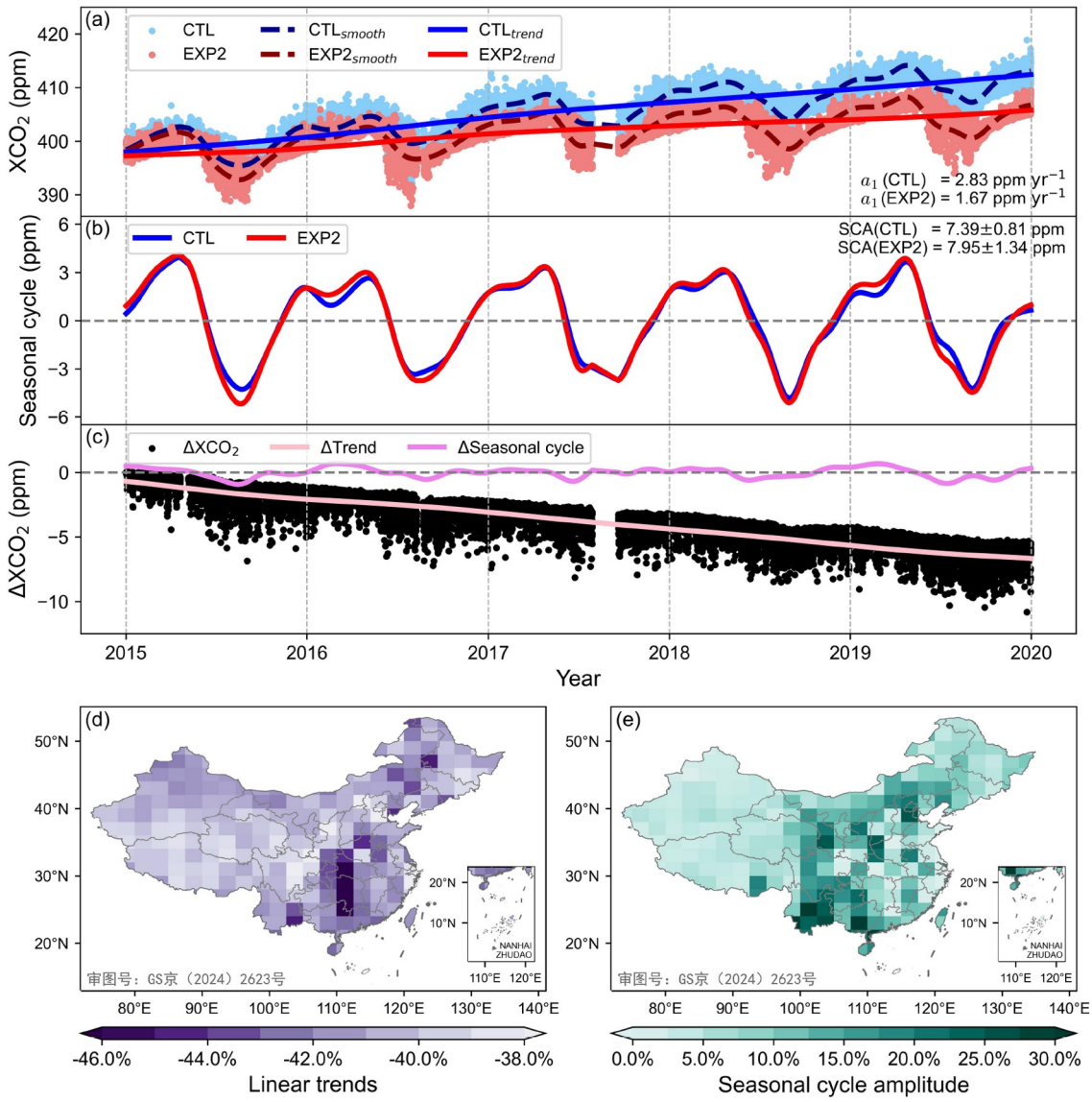

Figure 6 XCO_2 changes in China under zero fossil CO_2 emissions (EXP2). (a) The original values, smoothed fitted curves, and trend lines of XCO_2 in CTL (blue dots and lines) and EXP2 (red dots and lines); (b) seasonal cycle of XCO_2 in CTL (blue line) and EXP2 (red line); (c) difference in XCO_2 between EXP2 and CTL; (d) relative changes in trends of XCO_2 between EXP2 and CTL; (e) relative changes in the SCA of XCO_2.

Table 2 Changes in trends (a_1) and seasonal cycle amplitude (SCA) of CO_2 concentrations in China relative to the control experiment

CO_2 concentrations	Locations	Changes	EXP1	EXP2	EXP3
XCO_2	China	a_1	−35.89%	−40.81%	4.92%
		SCA	−9.91%	7.57%	−16.61%
Surface CO_2	WLG	a_1	−41.88%	−47.85%	6.11%
		SCA	−20.36%	24.10%	−32.88%
	LFS	a_1	−54.37%	−37.60%	−16.66%
		SCA	−58.82%	−6.49%	−49.31%
	LAN	a_1	−44.64%	−46.63%	1.89%
		SCA	−57.93%	−32.32%	−28.08%
	XGL	a_1	−34.59%	−49.41%	15.04%
		SCA	−35.21%	12.30%	−45.92%

In contrast, Figure 7 demonstrates the impact of zero terrestrial CO_2 sinks in China (EXP3). Absence of terrestrial CO_2 sinks results in the linear trends of 2.97 ppm yr^{-1} (p<0.01) in XCO_2 in China, showing a slight increase of 0.14 ppm yr^{-1} compared to that in CTL. Consequently, China's terrestrial CO_2 sinks mitigate the increasing trend in XCO_2 by approximately 4.92%, although this effect is much smaller than that of fossil CO_2 emissions. Conversely, terrestrial CO_2 sinks contribute to an enhanced SCA by 1.23 ppm, or approximately 16.61% (nearly twice the effect of fossil CO_2 emissions).

Spatially, the absence of terrestrial CO_2 sinks leads to an increase in the linear trends of XCO_2 across China, especially in the western regions (Figure 7d). The mitigating effects are consistent with the overall expression of carbon sinks in China (Figure 1b), and the spatial pattern of annual XCO_2 increase was generally consistent with the vegetated areas (Appendix Figure S4k–S4o). However, terrestrial CO_2 sinks peak in summer in the eastern part of China (Figure 1b), coinciding with prevailing southwesterly and southeasterly winds associated with the East Asian summer monsoon (Appendix Figure S2b), blowing atmospheric CO_2 inland. Consequently, stronger reductions in XCO_2 trends are observed in the western part of China under the effect of multi-year accumulation (Figure 7d and Appendix Figure S7i–S7l). Conversely, the spatial pattern of SCA without terrestrial

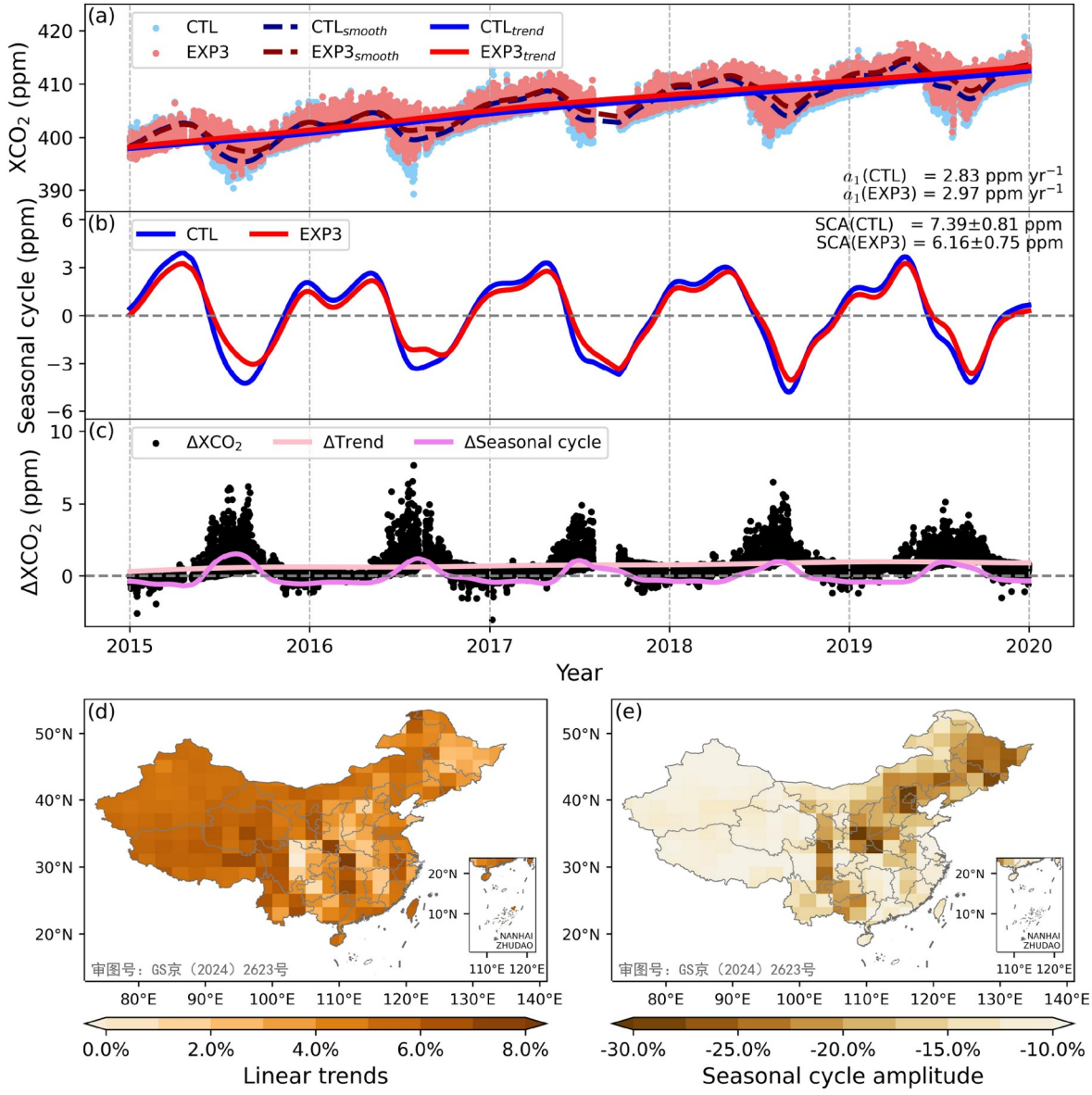

Figure 7 XCO_2 changes in China under zero terrestrial CO_2 sinks (EXP3). (a) The original values, smoothed fitted curves, and trend lines of XCO_2 in CTL (blue dots and lines) and EXP3 (red dots and lines); (b) seasonal cycle of XCO_2 in CTL (blue line) and EXP3 (red line); (c) difference in XCO_2 between EXP3 and CTL; (d) relative changes in trends of XCO_2 between EXP3 and CTL; (e) relative changes in the SCA of XCO_2.

CO_2 sinks resembles the pattern under ideal net-zero emissions (Figure 5b).

3.4 Surface CO_2 concentration changes under ideal net-zero emissions

Figure 8 shows the simulated surface CO_2 concentrations under ideal net-zero emissions for four stations: WLG, LFS, LAN, and XGL, and simulated concentrations for JSA and SDZ in Appendix Figure S8. Compared to the linear trends of 2.96 ppm yr^{-1} and the SCA of 10.06±2.67 ppm at WLG in CTL, net-zero emissions result in variations of surface CO_2 concentrations, decreasing to 1.72 and 8.01±0.31 ppm, respectively. Thus, the surface CO_2 concentration at the atmospheric background baseline monitoring site WLG has seen a reduction of 6.6 ppm from 2015 to 2019, similar to the accumulated reduction of 5.39 ppm in XCO_2 (Figure 4a). Relatively, China's net-zero CO_2 emissions result in a decrease of approximately 41.88% in the increasing CO_2 concentration at WLG, with fossil CO_2 emissions and terrestrial

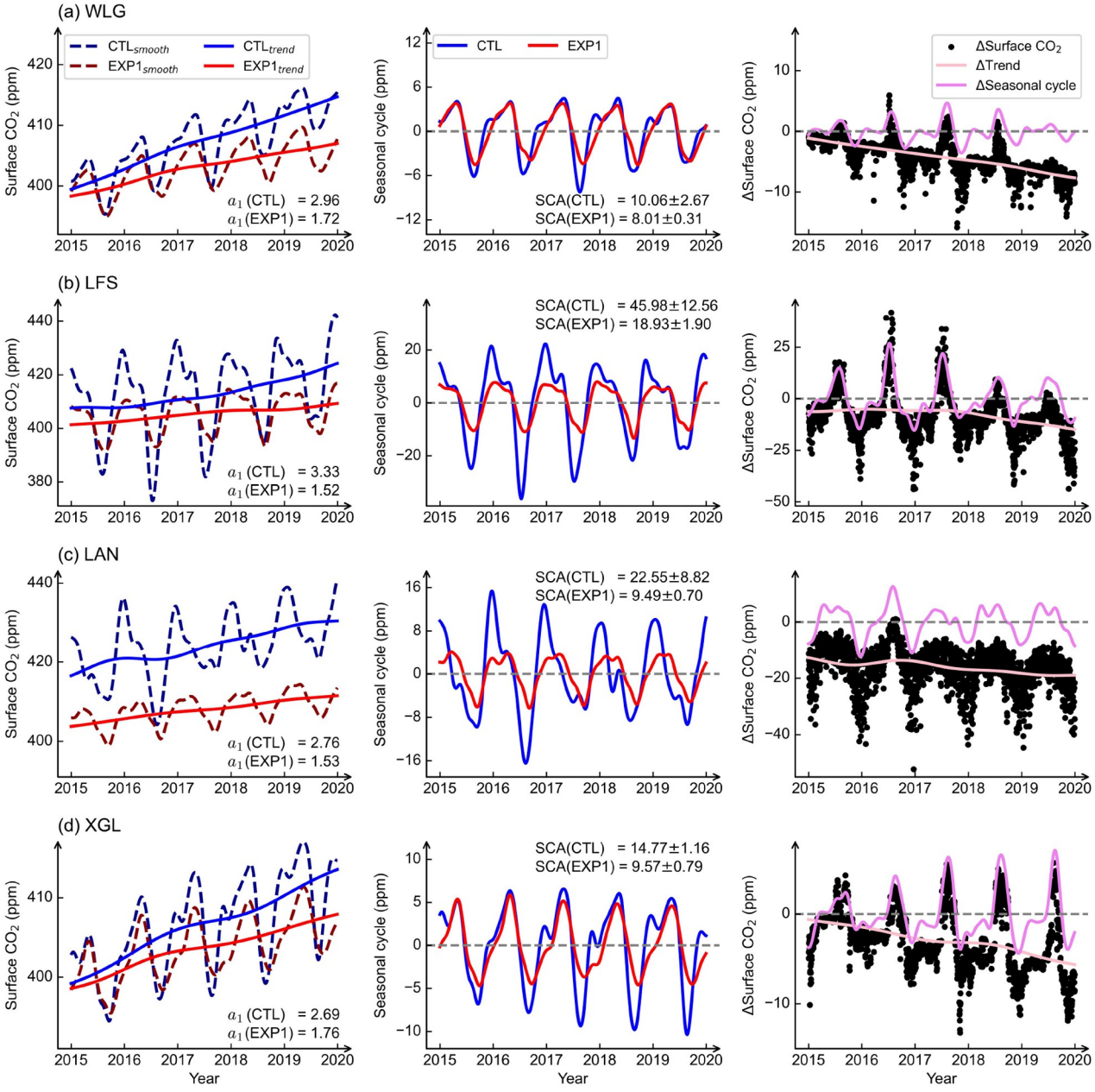

Figure 8 Changes of surface CO_2 in the trend and SCA under the ideal net-zero CO_2 emissions are four stations for WLG (a), LFS (b), LAN (c), and XGL (d). The left column is the smoothed fitted curves (dashed lines) and the trend line (solid line) in CTL (blue) and EXP1 (red). The center column is their seasonal cycle. The right column is the difference between the two scenarios, including magnitudes (dots), trends (pink line), and seasonal cycles (purple line). The unit of a_1 is ppm yr^{-1} and the unit of SCA is ppm.

CO_2 sinks accounting for −47.85% and 6.11%, respectively (Table 2). In addition, net-zero CO_2 emissions substantially reduce the SCA by 20.36%, a much stronger effect than that observed in XCO_2. Individually, zero fossil CO_2 emissions lead to a 24.10% increase in SCA, while the absence of terrestrial CO_2 sinks causes a significant 32.88% reduction in SCA.

At the LFS and XGL stations, the trends and seasonal cycles of surface CO_2 concentrations are similar to those at the WLG station (Figure 8b and 8d). Under net-zero CO_2 emissions, reductions in increasing CO_2 concentrations are consistently dominated by fossil CO_2 emissions, accounting for −37.60% and −49.41%, respectively. Meanwhile, reductions in the SCA are both driven by terrestrial CO_2 sinks, explaining −49.31% and −45.92%, respectively.

At last, the LAN station, situated in the Yangtze River Delta, a region with high fossil CO_2 emissions, behaves somewhat differently. Net-zero CO_2 emissions result in an accumulated reduction in surface CO_2 concentration of 15 ppm, much larger than the other three stations. Compared with 2.76 ppm yr^{-1} in CTL, the linear trend in net-zero emissions is reduced to 1.53 ppm yr^{-1}, a decrease of 44.64%. The seasonal cycle also varies significantly, with SCA reduced by 57.93% to 9.49±0.70 ppm under net-zero emissions compared with 22.55±8.82 ppm in CTL. However, its SCA reduction is dominated by fossil CO_2 emissions (−32.32%) rather than terrestrial CO_2 sinks (−28.08%).

In general, under the net-zero CO_2 emissions, reductions in trends of surface CO_2 concentrations at stations are comparable to the reduction in XCO_2 in China (Table 2). However, reductions in the SCA of surface CO_2 concentrations at stations exhibit a much stronger magnitude than that in XCO_2, suggesting that variations in surface CO_2 concentrations are more susceptible to changes in surface carbon sources and sinks on a shorter time-scale.

4. Conclusion and discussion

We in this study investigated the impact of ideal net-zero CO_2 emissions on XCO_2 and surface CO_2 concentrations in China through sensitivity experiments using the GEOS-Chem model for the period from 2015 to 2019. GEOS-Chem provides an effective reproduction of atmospheric CO_2 concentrations, simulating an RMSE of 1.51 ppm (R^2=0.89) for XCO_2 with OCO-2 observations and an RMSE of 2.65 ppm (R^2=0.75) for surface CO_2 concentrations with observations of the WLG station. Compared with results in CTL, the increasing trend of XCO_2 under net-zero emissions decreases from 2.83 to 1.81 ppm yr^{-1}, representing a reduction of 1.02 ppm yr^{-1}. This results in a cumulative reduction of 5.39 ppm in XCO_2 over five years. Relatively, China's net-zero CO_2 emissions reduce the increasing trend of XCO_2 by 35.89%, primarily driven by a reduction of fossil CO_2 emissions (−40.81%). In addition, the change in the SCA of XCO_2 is less pronounced, decreasing from 7.39±0.70 ppm in CTL to 6.75±0.70 ppm, a relative reduction of 9.91%. Spatially, stronger reductions in trends of XCO_2 are observed over northern and southern China, while northern and northeastern China experiences a more significant decrease in the SCA.

Furthermore, we find that surface CO_2 concentrations are more susceptible to changes in CO_2 sources and sinks. Under China's net-zero CO_2 emissions, the growth of surface concentrations significantly slow, even with a reduction of 54.37% at the LFS station. Additionally, the LAN station, located in a high fossil CO_2 emission region, reflects a more dramatic decrease in surface CO_2 concentration (approximately 15 ppm) compared with the other three stations (WLG, LFS, and XGL). Meanwhile, the SCA of surface CO_2 concentration is markedly reduced by net-zero CO_2 emissions, more than twice the reduction observed in XCO_2.

It is worth noting that uncertainties exist in these model simulations, primarily stemming from three sources: input data for surface fluxes, restart files, and errors in the atmospheric transport model (Fu et al., 2019; Schuh et al., 2019; Liu et al., 2024). To reduce these uncertainties, we have taken several measures. For example, we used surface fluxes from ODIAC, as prescribed in the OCO-2 v10 MIP (Oda et al., 2018; Byrne et al., 2023), and the optimized results from GCASv2 (Wang et al., 2019; Jiang et al., 2021). The required restart file was generated from a one-year spin-up based on an assimilation study. In addition, the GEOS-Chem model, a widely recognized global atmospheric chemistry model, was used due to its proven accuracy in simulating CO_2 concentrations (Zhang et al., 2017; Mustafa et al., 2021; Allahudheen et al., 2023; Su et al., 2023).

Overall, these ideal simulations imply that China's commitment to achieving net-zero CO_2 emissions represents a significant stride towards mitigating the escalating concentrations of atmospheric CO_2 and addressing climate change. China's carbon neutrality goal will play a crucial role in slowing the progression of global warming. However, it is important to recognize that while China's efforts to achieve net-zero CO_2 emissions can mitigate a substantial portion—approximately 35.89%—of the rising XCO_2 trend, it alone is insufficient to effectively combat climate change. Additionally, carbon emissions from other countries can impact CO_2 concentrations in China via atmospheric transport. For instance, the WLG station, influenced by the westerly wind belt, shows high sensitivity to surface emissions in Eurasia (Cheng et al., 2017). Therefore, to better address the challenges of global warming and strive to limit the rise in global temperatures to 1.5°C (Rogelj et al., 2016; Roelfsema et al., 2020), concerted and collaborative efforts from nations worldwide are imperative.

Despite the commendable strides towards carbon neutrality, it is essential to note that the carbon neutrality proposed by various nations does not inherently lead to a reduction in atmospheric CO_2 levels. Achieving net-negative CO_2 emissions is necessary, requiring the implementation of measures such as CCUS (Chen et al., 2022; Shang and Lv, 2023), among others.

Moreover, it is noteworthy that the primary pathway to achieving net-zero CO_2 emissions involves both reducing fossil CO_2 emissions and enhancing natural CO_2 sinks. Through the idealized experiments outlined in this study (Figures 4, 6, and 7), it is projected that while the upward trend in CO_2 concentrations diminishes under such implementation pathways, the SCA is anticipated to change obviously. Understanding the variation in SCA is a focal point in some recent literatures (Zeng et al., 2014; Wang et al., 2021).

Acknowledgements *XCO_2 dataset from OCO-2 is available at https://disc.gsfc.nasa.gov/datasets/OCO2_L2_Lite_FP_10r/summary. Surface CO_2 dataset form ObsPack is available at https://gml.noaa.gov/ccgg/obspack/data.php. GCAS is available at http://www.gcas.net.cn/gcasPages/dataDownload/dataDownload.html. This study was supported by the National Key Research and Development Program of China (Grant No. 2022YFB3904801), the National Natural Science Foundation of China (Grant No. 42475129), the Natural Science Foundation of Jiangsu Province, China (Grant No. BK20221449), the Xizang Science and Technology Innovation Base Construction Project (Grant No. XZ202401YD0008), and the National Key Scientific and Technological Infrastructure project "Earth System Numerical Simulation Facility" (Grant No. 2023-EL-ZD-00022).*

Conflict of interest The authors declare that they have no conflict of interest.

References

AghaKouchak A, Chiang F, Huning L S, Love C A, Mallakpour I, Mazdiyasni O, Moftakhari H, Papalexiou S M, Ragno E, Sadegh M. 2020. Climate extremes and compound hazards in a warming world. Annu Rev Earth Planet Sci, 48: 519–548

Allahudheen S, Chandra A B, Nayak R K, Dadhwal V K, Krishnapriya M, Lakshmaiah M V. 2023. High-resolution GEOS-Chem model for Indian monsoon region: Seasonal cycle and budget of tropospheric CO_2. Atmos Environ, 309: 119913

Bukosa B, Fisher J A, Deutscher N M, Jones D B A. 2023. A coupled CH_4, CO and CO_2 simulation for improved chemical source modeling. Atmosphere, 14: 764

Byrne B, Baker D F, Basu S, Bertolacci M, Bowman K W, Carroll D, Chatterjee A, Chevallier F, Ciais P, Cressie N, Crisp D, Crowell S, Deng F, Deng Z, Deutscher N M, Dubey M K, Feng S, García O E, Griffith D W T, Herkommer B, Hu L, Jacobson A R, Janardanan R, Jeong S, Johnson M S, Jones D B A, Kivi R, Liu J J, Liu Z Q, Maksyutov S, Miller J B, Miller S M, Morino I, Notholt J, Oda T, O'Dell C W, Oh Y S, Ohyama H, Patra P K, Peiro H, Petri C, Philip S, Pollard D F, Poulter B, Remaud M, Schuh A, Sha M K, Shiomi K, Strong K, Sweeney C, Té Y, Tian H Q, Velazco V A, Vrekoussis M, Warneke T, Worden J R, Wunch D, Yao Y Z, Yun J, Zammit-Mangion A, Zeng N. 2023. National CO_2 budgets (2015–2020) inferred from atmospheric CO_2 observations in support of the global stocktake. Earth Syst Sci Data, 15: 963–1004

Chatterjee A, Gierach M M, Sutton A J, Feely R A, Crisp D, Eldering A, Gunson M R, O'Dell C W, Stephens B B, Schimel D S. 2017. Influence of El Niño on atmospheric CO_2 over the tropical Pacific Ocean: Findings from NASA's OCO-2 mission. Science, 358: eaam5776

Chen S, Liu J, Zhang Q, Teng F, McLellan B C. 2022. A critical review on deployment planning and risk analysis of carbon capture, utilization, and storage (CCUS) toward carbon neutrality. Renew Sust Energy Rev, 167: 112537

Cheng S Y, An X Q, Zhou L X, Tans P P, Jacobson A. 2017. Atmospheric CO_2 at Waliguan station in China: Transport climatology, temporal patterns and source-sink region representativeness. Atmos Environ, 159: 107–116

Connor B J, Boesch H, Toon G, Sen B, Miller C, Crisp D. 2008. Orbiting Carbon Observatory: Inverse method and prospective error analysis. J Geophys Res, 113: 2006JD008336

Dong H M, Liu Y S, Zhao Z H, Tan X J, Managi S. 2022. Carbon neutrality commitment for China: From vision to action. Sust Sci, 17: 1741–1755

Eldering A, Wennberg P O, Crisp D, Schimel D S, Gunson M R, Chatterjee A, Liu J, Schwandner F M, Sun Y, O'Dell C W, Frankenberg C, Taylor T, Fisher B, Osterman G B, Wunch D, Hakkarainen J, Tamminen J, Weir B. 2017. The Orbiting Carbon Observatory-2 early science investigations of regional carbon dioxide fluxes. Science, 358: eaam5745

Feldman A F, Zhang Z, Yoshida Y, Chatterjee A, Poulter B. 2023. Using Orbiting Carbon Observatory-2 (OCO-2) column CO_2 retrievals to rapidly detect and estimate biospheric surface carbon flux anomalies. Atmos Chem Phys, 23: 1545–1563

Fu Y, Liao H, Tian X J, Gao H, Cai Z N, Han R. 2019. Sensitivity of the simulated CO_2 concentration to inter-annual variations of its sources and sinks over East Asia. Adv Clim Change Res, 10: 250–263

Fuglestvedt J, Rogelj J, Millar R J, Allen M, Boucher O, Cain M, Forster P M, Kriegler E, Shindell D. 2018. Implications of possible interpretations of 'greenhouse gas balance' in the Paris Agreement. Phil Trans R Soc A, 376: 20160445

Gampe D, Zscheischler J, Reichstein M, O'Sullivan M, Smith W K, Sitch S, Buermann W. 2021. Increasing impact of warm droughts on northern ecosystem productivity over recent decades. Nat Clim Chang, 11: 772–779

He Y G, Li X, Huang P P, Wang J N. 2022. Exploring the road toward environmental sustainability: Natural resources, renewable energy consumption, economic growth, and greenhouse gas emissions. Sustainability, 14: 1579

Hoesly R M, Smith S J, Feng L Y, Klimont Z, Janssens-Maenhout G, Pitkanen T, Seibert J J, Vu L, Andres R J, Bolt R M, Bond T C, Dawidowski L, Kholod N, Kurokawa J-I, Li M, Liu L, Lu Z F, Moura M C P, O'Rourke P R, Zhang Q. 2018. Historical (1750–2014) anthropogenic emissions of reactive gases and aerosols from the Community Emissions Data System (CEDS). Geosci Model Dev, 11: 369–408

Höök M, Tang X. 2013. Depletion of fossil fuels and anthropogenic climate change—A review. Energy Policy, 52: 797–809

IPCC. 2021. Climate Change 2021. The Physical Science Basis. Contribution of Working Group I to the Sixth Assessment Report of the Intergovernmental Panel on Climate Change. Cambridge: Cambridge University Press, 2021. 425–427

Jeffry L, Ong M Y, Nomanbhay S, Mofijur M, Mubashir M, Show P L. 2021. Greenhouse gases utilization: A review. Fuel, 301: 121017

Jiang F, Wang H M, Chen J M, Ju W M, Tian X J, Feng S Z, Li G C, Chen Z Q, Zhang S P, Lu X H, Liu J, Wang H K, Wang J, He W, Wu M S. 2021. Regional CO_2 fluxes from 2010 to 2015 inferred from GOSAT XCO_2 retrievals using a new version of the Global Carbon Assimilation System. Atmos Chem Phys, 21: 1963–1985

Jin C L, Xue Y, Jiang X X, Zhao L, Yuan T, Sun Y X, Wu S H, Wang X K. 2022. A long-term global XCO_2 dataset: Ensemble of satellite products. Atmos Res, 279: 106385

Keenan T F, Prentice I C, Canadell J G, Williams C A, Wang H, Raupach M, Collatz G J. 2016. Recent pause in the growth rate of atmospheric CO_2 due to enhanced terrestrial carbon uptake. Nat Commun, 7: 13428

Keller C A, Long M S, Yantosca R M, Da Silva A M, Pawson S, Jacob D J.

2014. HEMCO v1.0: A versatile, ESMF-compliant component for calculating emissions in atmospheric models. Geosci Model Dev, 7: 1409–1417
Schuldt K N, Mund J, Luijkx I T, Aalto T, Abshire J B, Aikin K, et al. 2022. Multi-laboratory compilation of atmospheric carbon dioxide data for the period 1957–2021; obspack_co2_1_GLOBALVIEWplus_v8.0_2022-08-27
Kiel M, O'Dell C W, Fisher B, Eldering A, Nassar R, MacDonald C G, Wennberg P O. 2019. How bias correction goes wrong: Measurement of XCO_2 affected by erroneous surface pressure estimates. Atmos Meas Tech, 12: 2241–2259
Laufkötter C, Zscheischler J, Frölicher T L. 2020. High-impact marine heatwaves attributable to human-induced global warming. Science, 369: 1621–1625
Li B P, Gasser T, Ciais P, Piao S, Tao S, Balkanski Y, Hauglustaine D, Boisier J P, Chen Z, Huang M T, Li L Z X, Li Y, Liu H Y, Liu J F, Peng S S, Shen Z H, Sun Z Z, Wang R, Wang T, Yin G D, Yin Y, Zeng H, Zeng Z Z, Zhou F. 2016. The contribution of China's emissions to global climate forcing. Nature, 531: 357–361
Li J, Jia K, Wei X Q, Xia M, Chen Z L, Yao Y J, Zhang X T, Jiang H Y, Yuan B, Tao G F, Zhao L L. 2022. High-spatiotemporal resolution mapping of spatiotemporally continuous atmospheric CO_2 concentrations over the global continent. Int J Appl Earth Observat Geoinf, 108: 102743
Lin H, Jacob D J, Lundgren E W, Sulprizio M P, Keller C A, Fritz T M, Eastham S D, Emmons L K, Campbell P C, Baker B, Saylor R D, Montuoro R. 2021. Harmonized Emissions Component (HEMCO) 3.0 as a versatile emissions component for atmospheric models: Application in the GEOS-Chem, NASA GEOS, WRF-GC, CESM2, NOAA GEFS-Aerosol, and NOAA UFS models. Geosci Model Dev, 14: 5487–5506
Liu Z, Zeng N, Liu Y, Wang J, Han P F, Cai Q X. 2024. Weaker regional carbon uptake albeit with stronger seasonal amplitude in northern mid-latitudes estimated by higher resolution GEOS-Chem model. Sci Total Environ, 912: 169477
Lou H Z, Shi X W, Ren X Y, Yang S T, Cai M Y, Pan Z H, Zhu Y F, Feng D Y, Zhou B C. 2024. Limited terrestrial carbon sinks and increasing carbon emissions from the Hu Line spatial pattern perspective in China. Ecol Indicators, 162: 112035
Masarie K A, Peters W, Jacobson A R, Tans P P. 2014. ObsPack: A framework for the preparation, delivery, and attribution of atmospheric greenhouse gas measurements. Earth Syst Sci Data, 6: 375–384
Messerschmidt J, Parazoo N, Wunch D, Deutscher N M, Roehl C, Warneke T, Wennberg P O. 2013. Evaluation of seasonal atmosphere-biosphere exchange estimations with TCCON measurements. Atmos Chem Phys, 13: 5103–5115
Mustafa F, Wang H J, Bu L B, Wang Q, Shahzaman M, Bilal M, Zhou M Q, Iqbal R, Aslam R W, Ali M A, Qiu Z F. 2021. Validation of GOSAT and OCO-2 against *in situ* aircraft measurements and comparison with CarbonTracker and GEOS-Chem over Qinhuangdao, China. Remote Sens, 13: 899
Oda T, Maksyutov S. 2011. A very high-resolution (1 km×1 km) global fossil fuel CO_2 emission inventory derived using a point source database and satellite observations of nighttime lights. Atmos Chem Phys, 11: 543–556
Oda T, Maksyutov S, Andres R J. 2018. The Open-source Data Inventory for Anthropogenic CO_2, version 2016 (ODIAC2016): A global monthly fossil fuel CO_2 gridded emissions data product for tracer transport simulations and surface flux inversions. Earth Syst Sci Data, 10: 87–107
Olsen S C, Wuebbles D J, Owen B. 2013. Comparison of global 3-D aviation emissions datasets. Atmos Chem Phys, 13: 429–441
Ponce P, Khan S A R. 2021. A causal link between renewable energy, energy efficiency, property rights, and CO_2 emissions in developed countries: A road map for environmental sustainability. Environ Sci Pollut Res, 28: 37804–37817
Press W H, Teukolsky S A, Vetterling W T, Flannery B P. 1988. Numerical Recipes in C: The Art of Scientific Computing. Cambridge: Cambridge University Press
Randerson J T, van der Werf G R, Giglio L, Collatz G J, Kasibhatla P S. 2018. Global Fire Emissions Database, Version 4.1 (GFEDv4). Oak Ridge: ORNL DAAC
Roelfsema M, van Soest H L, Harmsen M, van Vuuren D P, Bertram C, den Elzen M, Höhne N, Iacobuta G, Krey V, Kriegler E, Luderer G, Riahi K, Ueckerdt F, Després J, Drouet L, Emmerling J, Frank S, Fricko O, Gidden M, Humpenöder F, Huppmann D, Fujimori S, Fragkiadakis K, Gi K, Keramidas K, Köberle A C, Aleluia Reis L, Rochedo P, Schaeffer R, Oshiro K, Vrontisi Z, Chen W Y, Iyer G C, Edmonds J, Kannavou M, Jiang K J, Mathur R, Safonov G, Vishwanathan S S. 2020. Taking stock of national climate policies to evaluate implementation of the Paris Agreement. Nat Commun, 11: 2096
Rogelj J, den Elzen M, Höhne N, Fransen T, Fekete H, Winkler H, Schaeffer R, Sha F, Riahi K, Meinshausen M. 2016. Paris Agreement climate proposals need a boost to keep warming well below 2 °C. Nature, 534: 631–639
Rogelj J, Huppmann D, Krey V, Riahi K, Clarke L, Gidden M, Nicholls Z, Meinshausen M. 2019. A new scenario logic for the Paris Agreement long-term temperature goal. Nature, 573: 357–363
Salvia M, Reckien D, Pietrapertosa F, Eckersley P, Spyridaki N A, Krook-Riekkola A, Olazabal M, De Gregorio Hurtado S, Simoes S G, Geneletti D, Viguié V, Fokaides P A, Ioannou B I, Flamos A, Csete M S, Buzasi A, Orru H, de Boer C, Foley A, Rižnar K, Matosović M, Balzan M V, Smigaj M, Baštáková V, Streberova E, Šel N B, Coste L, Tardieu L, Altenburg C, Lorencová E K, Orru K, Wejs A, Feliu E, Church J M, Grafakos S, Vasilie S, Paspaldzhiev I, Heidrich O. 2021. Will climate mitigation ambitions lead to carbon neutrality? An analysis of the local-level plans of 327 cities in the EU. Renew Sust Energy Rev, 135: 110253
Schuh A E, Jacobson A R, Basu S, Weir B, Baker D, Bowman K, Chevallier F, Crowell S, Davis K J, Deng F, Denning S, Feng L, Jones D, Liu J, Palmer P I. 2019. Quantifying the impact of atmospheric transport uncertainty on CO_2 surface flux estimates. Glob Biogeochem Cycle, 33: 484–500
Shang W L, Lv Z H. 2023. Low carbon technology for carbon neutrality in sustainable cities: A survey. Sustain Cities Soc, 92: 104489
Su M Q, Shi Y S, Yang Y L, Guo W Y. 2023. Impacts of different biomass burning emission inventories: Simulations of atmospheric CO_2 concentrations based on GEOS-Chem. Sci Total Environ, 876: 162825
Thoning K W, Tans P P, Komhyr W D. 1989. Atmospheric carbon dioxide at Mauna Loa Observatory: 2. Analysis of the NOAA GMCC data, 1974–1985. J Geophys Res, 94: 8549–8565
van Soest H L, den Elzen M G J, van Vuuren D P. 2021. Net-zero emission targets for major emitting countries consistent with the Paris Agreement. Nat Commun, 12: 2140
Vicedo-Cabrera A M, Scovronick N, Sera F, Royé D, Schneider R, Tobias A, Astrom C, Guo Y, Honda Y, Hondula D M, Abrutzky R, Tong S, de Sousa Zanotti Stagliorio Coelho M, Saldiva P H N, Lavigne E, Correa P M, Ortega N V, Kan H, Osorio S, Kyselý J, Urban A, Orru H, Indermitte E, Jaakkola J J K, Ryti N, Pascal M, Schneider A, Katsouyanni K, Samoli E, Mayvaneh F, Entezari A, Goodman P, Zeka A, Michelozzi P, de'Donato F, Hashizume M, Alahmad B, Diaz M H, Valencia C D L C, Overcenco A, Houthuijs D, Ameling C, Rao S, Di Ruscio F, Carrasco-Escobar G, Seposo X, Silva S, Madureira J, Holobaca I H, Fratianni S, Acquaotta F, Kim H, Lee W, Iniguez C, Forsberg B, Ragettli M S, Guo Y L L, Chen B Y, Li S, Armstrong B, Aleman A, Zanobetti A, Schwartz J, Dang T N, Dung D V, Gillett N, Haines A, Mengel M, Huber V, Gasparrini A. 2021. The burden of heat-related mortality attributable to recent human-induced climate change. Nat Clim Chang, 11: 492–500
Wang H M, Jiang F, Wang J, Ju W M, Chen J M. 2019. Terrestrial ecosystem carbon flux estimated using GOSAT and OCO-2 XCO_2 retrievals. Atmos Chem Phys, 19: 12067–12082
Wang J, Liu Z Q, Zeng N, Jiang F, Wang H M, Ju W M. 2020. Spaceborne detection of XCO_2 enhancement induced by Australian mega-bushfires. Environ Res Lett, 15: 124069

Wang K, Wang X H, Piao S L, Chevallier F, Mao J F, Shi X Y, Huntingford C, Bastos A, Ciais P, Xu H, Keeling R F, Pacala S W, Chen A P. 2021. Unusual characteristics of the carbon cycle during the 2015−2016 El Niño. Glob Change Biol, 27: 3798–3809
Williams J H, Jones R A, Haley B, Kwok G, Hargreaves J, Farbes J, Torn M S. 2021. Carbon-neutral pathways for the United States. AGU Adv, 2: e2020AV000284
WMO. 2023. WMO Greenhouse Gas Bulletin No. 19. World Meteorological Organization
Zeng N, Zhao F, Collatz G J, Kalnay E, Salawitch R J, West T O, Guanter L. 2014. Agricultural Green Revolution as a driver of increasing atmospheric CO_2 seasonal amplitude. Nature, 515: 394–397
Zhang L L, Yue T X, Wilson J P, Zhao N, Zhao Y P, Du Z P, Liu Y. 2017. A comparison of satellite observations with the XCO_2 surface obtained by fusing TCCON measurements and GEOS-Chem model outputs. Sci Total Environ, 601-602: 1575–1590
Zhang W X, Zhou T J. 2020. Increasing impacts from extreme precipitation on population over China with global warming. Sci Bull, 65: 243–252
Zhang Y X, Luo H L, Wang C. 2021. Progress and trends of global carbon neutrality pledges (in Chinese). Clim Change Res, 17: 88–97

(Editorial handling: Renhe ZHANG)